Nuclear Materials and Energy 34 (2023) 101375

Contents lists available at ScienceDirect

Nuclear Materials and Energy

journal homepage: www.elsevier.com/locate/nme

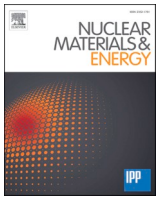

Thin films sputter-deposited from EUROFER97 in argon and deuterium atmosphere: Material properties and deuterium retention

E. Pitthan [a,*], P. Petersson [b], T.T. Tran [a], D. Moldarev [a], R. Kaur [a], J. Shams-Latifi [a], P. Ström [a], M. Hans [c], M. Rubel [a,b], D. Primetzhofer [a]

[a] Department of Physics and Astronomy, Ångström Laboratory, Uppsala University, Box 516, SE-751 20 Uppsala, Sweden
[b] Department of Fusion Plasma Physics, KTH Royal Institute of Technology, 10044, Stockholm, Teknikringen 31, Sweden
[c] Materials Chemistry, RWTH Aachen University, Kopernikusstraße 10, 52074 Aachen, Germany

ARTICLE INFO

Keywords:
Plasma facing components
EUROFER97
Sputtering deposition
Ion beam analysis
Deuterium retention

ABSTRACT

Sputter-deposited thin films (33–1160 nm) from EUROFER97 were obtained on different substrates (C, Si, W, MgO) in argon and a mix of argon and deuterium atmosphere. The composition, microstructure, and mechanical properties of the films were analyzed and compared to those of the bulk material. The films feature lower density (-10%), higher hardness (+79%), and smaller crystallites in comparison to the bulk. Despite such differences, the elemental atomic composition of the films and the bulk was very similar, as determined by ion beam analysis. Deposition in deuterium-containing atmosphere resulted in a low deuterium incorporation (0.28% of atomic content), indicating low retention of hydrogen-isotopes in the deposited material.

1. Introduction

EUROFER97 is a reduced activation ferritic-martensitic (RAFM) steel designed to be used for first wall and breeding blanket structural material in future nuclear fusion reactors. Tungsten-coated EUROFER97 is intended to be used for plasma-facing components (PFC) in a demonstration power plant, DEMO [1]. Uncoated RAFM steel is also considered for PFC in recessed areas of the first-wall due to technical (easier machining) and economic (lower cost) advantages in comparison to bulk tungsten (W) [2]. EUROFER97 presents a nominal atomic composition of 9.5 % Cr; 0.51 % C; 0.48 % Mn; 0.33 % W; 0.22 % V and 0.043 % Ta, and ≤0.02% of P, S, and Mo, balanced by Fe. The above numbers are converted from weight fractions published in [3]. PFC will be modified by plasma-wall interactions leading to a chain of steps in material migration i.e. erosion and re-deposition accompanied by co-deposition of species removed from the wall together with fuel atoms [4]. The latter process is decisive for fuel inventory in the wall and has a serious impact on the safety and economy in the reactor operation. In this context, several studies were conducted to investigate the modifications on EUROFER97 due to processes that will take place in fusion devices such as ion irradiation: it has been observed that the exposure of both EUROFER97 and Fe-W films (EUROFER model material) to low energy D ions leads to surface morphological changes including the enrichment of the surface region with W [1,5–9]. Similar enrichment was also reported as a result of thermally-induced segregation in EUROFER97 [10–12]. In addition to W and/or Ta, also Cr and S segregate at the surface of EUROFER97 upon annealing, as detected in recent studies [12]. In a consequence of the W enrichment and the modified surface nanostructure, the sputtering yield in such systems is reduced in comparison to pure Fe [13–15]. Surface enrichment with W was also observed for sputter-deposited Fe-W thin films subjected to both annealing and deuterium irradiation [10,16]. Capabilities for growing thin films with composition similar to bulk EUROFER97 would offer a deeper insight into the segregation (mobility) of Cr and minor constituents such as V, Ta and S. Additionally, film deposition on different substrates enables sputtering yield studies using quartz crystal microbalance (QCM) systems [17–18]. It also facilitates quantitative investigations of fundamental processes, e.g. energy loss of light ions in matter [19–20]. Such measurements are particularly important for EUROFER97 due to possible deviations from predictions based on the Bragg's rule, as it was found in alloys and compounds at low-to-middle energy regimes [21–22]. Finally, also in real fusion devices, re-deposited material will dominate on plasma facing areas – thus predicting its properties as well as a potential deviation from its bulk analogues is mandatory.

The simulation and assessment of effects related to material

* Corresponding author.
E-mail address: eduardo.pitthan@physics.uu.se (E. Pitthan).

https://doi.org/10.1016/j.nme.2023.101375
Received 28 November 2022; Received in revised form 13 January 2023; Accepted 23 January 2023
Available online 25 January 2023

migration under fusion-relevant conditions is the motivation for this work. We investigate how the properties of re-deposited layers differ from those of pristine bulk EUROFER97. There were three major objectives: (i) to obtain thin films sputter-deposited from the EUROFER97 target in argon (Ar) and in a mixed Ar-D_2 atmosphere; (ii) to examine morphology (composition, microstructure) and mechanical features of such layers in order to assess property differences between the original bulk material and the films; (iii) to quantify deuterium retention by the quantification and depth distribution of that isotope.

2. Materials and methods

The study was performed at the Tandem Laboratory at Uppsala University; a detailed description of the laboratory is given in [23]. Films were deposited using a PREVAC magnetron sputtering system equipped with two MS2 63C1 Magnetron sources suitable for targets with 50.8 mm (2 in.) diameter and 1–6 mm thickness. A 1 mm thick target was cut from a EUROFER97-3 (ID 46) block. The target thickness was minimized to reduce interference with the desired magnetic field of the magnetron cathode due to the ferromagnetic property of EUROFER97. Sputtered films were deposited at room temperature on four different substrates: glassy carbon (polished to nominal average roughness (R_a) < 50 nm), silicon wafer (Si), magnesium oxide (MgO (1 0 0) with nominal R_a < 0.5 nm) and polished W to allow the evaluation of homogeneity and composition including the detection of possible contaminants. The background pressure was below 8×10^{-6} Pa. Depositions in Ar atmosphere were performed using a gas flow rate of 10 standard cubic centimeter per minute (sccm), Ar pressure of 5.5×10^{-1} Pa, and a DC power of 50 W. Substrates were rotated with an angular frequency of 10°/s during deposition to increase the uniformity of the produced films. Pre-sputtering was performed against a shutter for 3–5 min before depositions to remove contaminants from the target surface. The deposition rate of 5.0 nm/min was initially estimated by QCM located in the sputtering system considering nominal density of Fe. Depositions in Ar and D_2 atmosphere were performed by mixing both gases before introduction into the chamber through the magnetron. Ar and D_2 flow was 10 and 18 sccm respectively, resulting in a pressure of 7.1×10^{-1} Pa (corresponding to 22.4% of D_2) and a deposition rate of 3.2 nm/min. To investigate possible isotopic exchange and outgassing effects, deposition under the same conditions was also performed using H_2 instead of D_2.

Material composition was determined by a set of complementary ion beam analysis (IBA) methods using a 5-MV NEC-5SDH-2 tandem accelerator (more details in [23]): Rutherford backscattering spectrometry (RBS), particle-induced X-ray emission (PIXE), time-of-flight elastic recoil detection analysis (ToF-ERDA), nuclear reaction analysis (NRA) and ERDA (i.e. without ToF). RBS and PIXE with a beam of 2 MeV He^+ primary ions were performed simultaneously using a passivated implanted planar silicon (PIPS) detector (scattering angle of 170°), and a silicon drift detector (SDD), respectively. RBS using 10 MeV $^{12}C^{3+}$ primary ions was also employed to achieve improved mass separation. The fits to RBS spectra were performed by SIMNRA code [24]. ToF-ERDA was carried out with a beam of 36 MeV $^{127}I^{8+}$ [25]. Data evaluation and depth profiles were obtained employing the CONTES code [26].

Deuterium quantification was done by NRA, using the $D(^3He,p)^4He$ reaction [27], with a 2 MeV $^3He^+$ primary beam at a normal incidence and a detection angle of 171° with respect to the primary beam. Normalization of the charge × solid angle product was performed using the RBS signal from the substrate. ERDA measurements with a primary beam of 2 MeV He^+ ions were conducted to obtain depth profiles of hydrogen isotopes in the samples. A solid-state detector was used at a forward scattering angle of 35° employing a collimator (area of 15.78 mm^2) to reduce angular straggling, resulting in a solid angle of 1.04 msr. A 9.1 μm mylar foil was placed in front of the detector for blocking of scattered and heavy recoiling-particles, thus enabling the detection of H and D recoils exclusively without a significant background. ERDA measurements at the incident angle of 70° were performed simultaneously with RBS which was used for charge normalization. ERDA and NRA data analysis was carried out with the SIMNRA software employing cross sections from SigmaCalc [28] for $^1H(\alpha,p)^4He$, from Besenbacher et al. for $D(^4He,D)^4He$ [29], and from Wielunska et al. for $D(^3He,p)^4He$ [27]. NRA combined with ERDA was used to analyze deuterium and hydrogen containing samples to minimize possible release of hydrogen isotopes during ToF-ERDA measurements [30].

For structural characterization the following techniques were employed: scanning electron (SEM), transmission electron (TEM) and atomic force microscopy (AFM), focused ion beam (FIB) and X-ray diffraction (XRD). TEM lamellae were produced by Zeiss FIB/SEM Crossbeam 550 with Ga Ion-Sculptor gun system. The region-of-interest areas of the films are selectively covered with a thin layer of platinum (Pt) to prevent these areas from being damaged by the Ga ions. TEM analysis was conducted with a FEI Titan Themis 200 system at an acceleration voltage of 200 kV. The surface topography of samples was studied by AFM in the contact mode using PSIA XE150 AFM, while the Gwyddion software [31] was employed for image processing. XRD was performed using a Siemens D5000 apparatus with a Cu-Kα radiation collimated using Göbel mirror. The incident angle was 10° to increase surface sensitivity and scans were carried out in steps of 0.02° (1 s per step) for 2θ ranging from 40° to 80°.

Load-controlled nanoindentation tests were conducted using a HysitronTI-900 TriboIndenter with a performech™ I Advanced Control Module. The maximum load of 2 mN was applied for each indent using a Berkovich diamond tip with a 100 nm radius. 36 indents (pattern of 6 × 6) with a distance of 5 μm between each indent were performed per sample, covering an area of 25 × 25 μm. The deviation of hardness and elastic modulus values within each nanoindentation dataset, obtained from 36 individual displacement curves, was <10%, hence, there was no strong roughness influence. The tip area was calibrated by indentation on fused silica before and after the measurements [32]. The elastic modulus was calculated considering a Poisson ratio equal to 0.3 [33]. A summary of all depositions and analysis performed in this work is presented in Table 1.

3. Results and discussion

Composition

Films were deposited for different times and on two types of substrates (C and Si) to allow evaluation of composition, and homogeneity. Rutherford backscattering spectra obtained with two different projectiles ($^4He^+$ and $^{12}C^{3+}$) for a film deposited for 5 min on the carbon substrate are shown Fig. 1 (a) and (b), respectively. The use of a carbon substrate permits detection of oxygen present in the film without signal interference from a heavier matrix, while the thin film (33 nm) allows for a better separation of the Cr and Fe signals. The spectrum obtained with a $^4He^+$ beam reveals signals of the transition metals, but Fe and Cr cannot be properly distinguished. Oxygen at the surface and interface is also observed, with no detectable oxygen in the bulk. Spectrum simulation indicates an atomic composition of 11% Cr, 88.7% Fe, and 0.3% W, being in good agreement with the nominal composition of bulk EUROFER97: 9.5% Cr, 88.9% Fe, and 0.33% W, as detailed in Introduction. A $^{12}C^{3+}$ beam was used to complement these measurements and to permit better separation between Cr and Fe; the result is shown in Fig. 1(b). Same atomic fraction of Cr, Fe, and W from the Fig. 1 (a) measurement was used in the simulation and resulted in a good agreement with experimental data, confirming the film composition. The presence of Ar in the film (atomic content of around 0.6%) was also observed. The presence of Ta in lower concentrations (0.043 %) is also expected but indistinguishable from W by RBS.

A thicker layer was deposited on Si to evaluate the film homogeneity, and the presence of light elements, e.g. carbon, in the bulk. Simulation of the spectrum using a thicker film and the same target composition as

Table 1
Parameters used for deposition of films using EUROFER97 as target; deposition rates deduced from QCM; substrates used; techniques used to analyze the resulting samples.

Atmosphere	Flux (sccm) Ar / D_2	P ($\times 10^{-1}$ Pa)	Deposition rate (nm/min)	Deposition time (min)	Substrates	Techniques
Ar	10	5.5	5.0	5	C	^{4}He-RBS; ^{12}C-RBS
Ar	10	5.5	5.0	60	C, Si	^{4}He-RBS/PIXE; ToF-ERDA; TEM
Ar	10	5.5	5.0	160	Si, MgO, W	^{4}He-RBS; AFM; XRD; nanoindentation
Ar + D_2	10/18	7.1	3.2	67	MgO	^{3}He-RBS/NRA; ^{4}He-RBS/ERDA

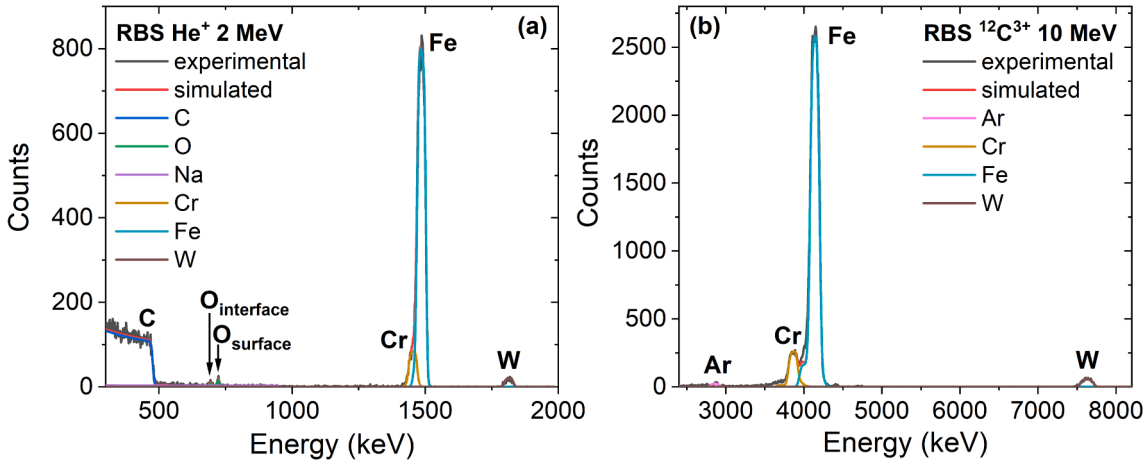

Fig. 1. RBS spectra from a EUROFER97 deposited film for 5 min under Ar atmosphere on a carbon substrate using as primary beam: (a) He^+ 2 MeV and (b) $^{12}C^{3+}$ 10 MeV.

previously described also resulted in a good agreement with experimental data. Considering the film density obtained experimentally (discussed in the following section), the film areal density in atoms/cm^2 corresponds to a film thickness of 350 nm. PIXE helped identification of constituents not easily detectable by RBS because of low concentrations and/or similar masses to other elements. PIXE spectra from the bulk material and deposited film on a Si substrate are shown for comparison in Fig. 2 (a). The results reveal excellent agreement between peaks originating from elements with $Z > Z(\mathrm{Si})$ in both targets. In addition to Cr, Fe and W, PIXE data confirm the presence of subtle amounts of V and Ta in the deposited films, with similar concentration as those found in the bulk sample. Finally, ToF-ERDA depth profiles presented in Fig. 2 (b) allow for the quantification of light contaminants. The result also proves high homogeneity of the film. Besides oxygen at the surface (also observed by RBS), the analyzed film contains in the bulk <1% of C, N, and O, while Cr + Fe and W average concentrations are 98.5 and 0.2% respectively (slightly lower W concentration in comparison to the 0.3% observed from RBS due to the presence of C, N, and O from ERDA).

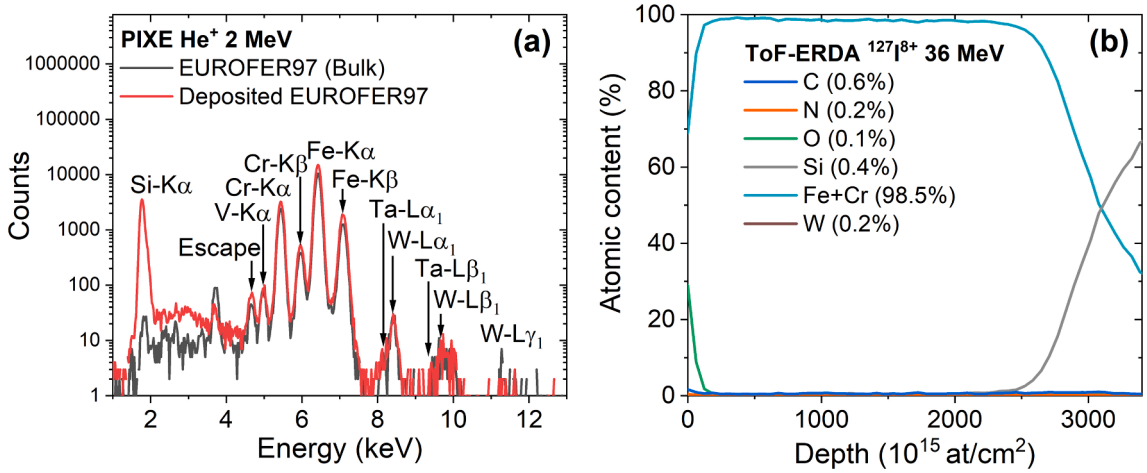

Fig. 2. PIXE spectrum (a) and ToF-ERDA depth profile (b) from a film deposited from EUROFER97 for 60 min under Ar atmosphere on a silicon substrate. A PIXE spectrum for a pristine EUROFER97 bulk is also added for comparison. The average atomic content presented as inset in depth profile is obtained in the depth interval from 800 to 1800 $\times$ 10^{15} atoms/cm^2.

3.2. Microstructure and mechanical properties

TEM micrographs for EUROFER97 bulk and deposited film on the C substrate during 60 min (resulting in a thickness of 371 nm) are presented in Fig. 3. Grains in irregular shapes and different sizes ranging from 25 nm up to 230 nm are observed in the bulk material, and were formed as a result of hot rolling and successive heat processing during manufacture [34–36]. The deposited films have columnar-like microstructure with a column width ranging from 25 nm to 80 nm. Such structure has been commonly observed in stainless steel and Fe films deposited by magnetron sputtering [37–38]. A film density of 6.99 g/cm^3 is calculated using the areal density obtained in RBS measurements and the layer thickness from TEM. This value is approximately 10 % lower than nominal EUROFER97 bulk value of 7.8460 g/cm^3 [12]. This result is quite typical for metallic films deposited by sputtering [39], and can be attributed to intra-and inter-columnar porosity. A root mean square roughness (R_q) of 7.8 nm was obtained from AFM images obtained for an area of 4 × 4 μm^2 from a surface of a film deposited for 160 min on a MgO substrate.

Fig. 4 presents the XRD patterns for EUROFER97 bulk and the films deposited on different substrates. Diffractograms for bulk and all types of films reveal the (1 1 0) and (0 0 2) α-Fe peaks from the bcc polycrystalline structure. From the analysis of (1 1 0) peaks, lattice parameter and mean crystallite size are calculated (Table 2). Very similar lattice parameters in all samples (bulk and films) strongly suggest similar crystal structure thus clearly indicating no influence of the substrate on the deposited film. Simultaneously, a significant reduction of mean crystallite size is observed in all deposited films in comparison to the bulk. The mean crystallite size deduced from XRD data differs from grain sizes observed in the lamellas by TEM. This difference can be understood based on the significantly different probing area from both techniques, and the fact that different crystallites (defined as coherent diffraction domain in the film) can be found within an individual grain [40]. Nevertheless, the difference in mean crystallite size between deposited films and bulk agrees with the different microstructures observed by TEM and, it can potentially result in different mechanical properties [36,41], as presented in the following.

Load-displacement curves in Fig. 5 were obtained for bulk metal polished to mirror-like finish to reduce the influence of surface roughness (process described in [12]), and for deposited films on different substrates. The extracted values for hardness and elastic modulus are presented in Table 2. Bulk values agree with those obtained by nanoindentation under similar displacement depth: 4.4 ± 0.4 GPa using a quasi-static method, and between 3.0 and 3.4 GPa using continuous stiffness measurement, both for a mean depth of 100 nm [42]. Lower hardness values are expected for higher loads (higher displacement

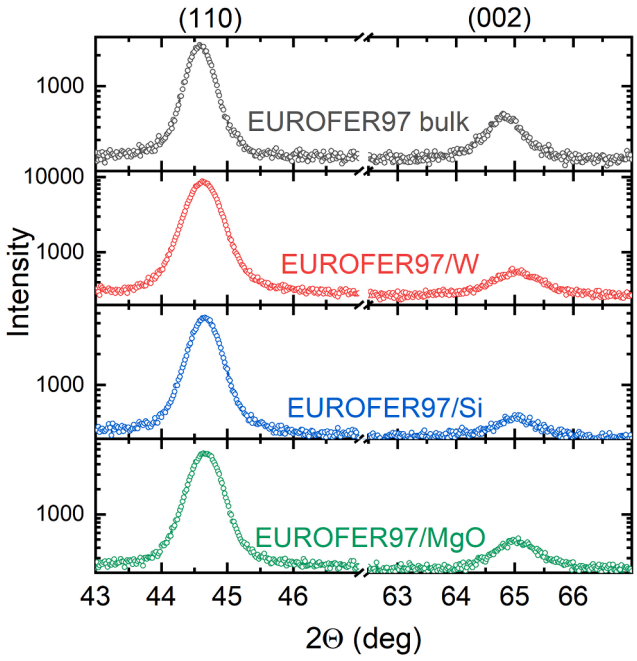

Fig. 4. XRD patterns from EUROFER 97 bulk and deposited films for 160 min under Ar atmosphere on different substrates.

Table 2
Lattice parameter and crystallite size calculated from XRD measurements (Fig. 4), and hardness and elastic modulus calculated from nanoindentation measurements (Fig. 5) for EUROFER 97 bulk and deposited films for 160 min under Ar atmosphere on different substrates.

Sample	Lattice parameter (Å)	Crystallite size (nm)	Hardness (GPa)	Elastic modulus (GPa)
EUROFER97 bulk	2.873 ± 0.009	38.1 ± 0.5	3.4 ± 0.2	240 ± 15
EUROFER97/W	2.870 ± 0.003	26.2 ± 0.1	6.4 ± 0.5	245 ± 15
EUROFER97/Si	2.869 ± 0.005	26.5 ± 0.2	6.5 ± 0.5	209 ± 13
EUROFER97/MgO	2.868 ± 0.004	28.8 ± 0.1	5.9 ± 0.4	231 ± 14

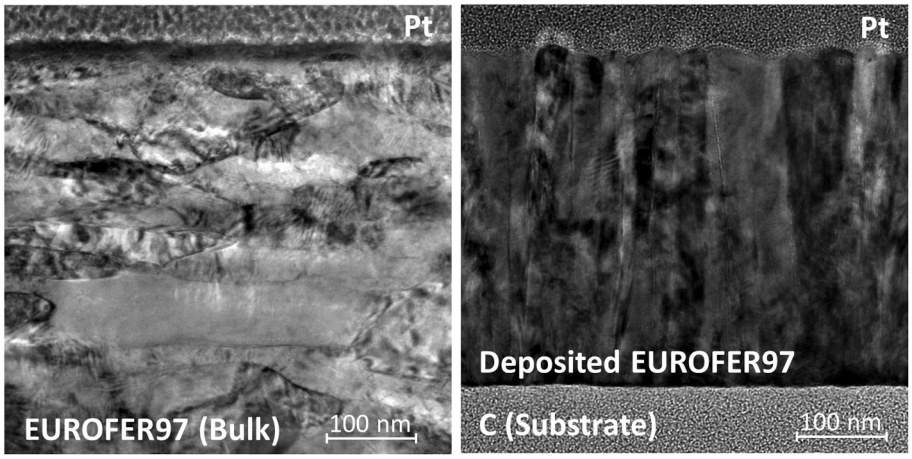

Fig. 3. TEM micrographs of a (top) EUROFER97 bulk, and a (bottom) EUROFER97 deposited film for 60 min under Ar atmosphere on a carbon substrate.

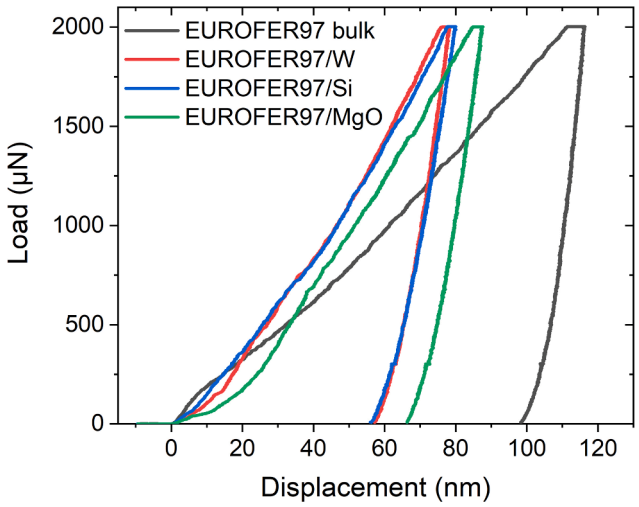

Fig. 5. Recorded load-displacement curves of EUROFER97 bulk and the films deposited for 160 min under Ar atmosphere on different substrates.

depths) due to the indentation size effect. A significantly lower displacement depth is observed in all films in comparison to the bulk (Fig. 5), although the imposed load function was identical. The hardness of deposited films on different substrates is significantly higher in comparison to the bulk. Such increase of hardness was previously measured on magnetron-sputtered stainless-steel films [43]. It is considered to be a result of smaller grains and crystallites, as observed also in the present study by TEM and XRD, respectively. On the other hand, similar elastic modulus has been found for most samples indicating similar stiffness of materials. The only exception is a lower elastic modulus value of the film deposited on Si, while the hardness is very similar to films deposited on W and MgO. The substrate effect on the hardness is negligible, when the indentation depth corresponds to 10% of the film thickness. However, since the elastic strain field radius is larger than the plastic zone radius, indentation depths of 2–3% have been recently suggested for measurements of the elastic modulus to avoid the substrate effect [44]. Hence, the smaller elastic modulus, measured for the film on Si is most likely affected by the substrate as the indentation depth corresponds to ~7% of the film thickness (indentation depth of 80 ± 4 nm and film thickness of 1100 nm).

3.3. Deuterium retention

Deuterium retention was evaluated in films produced by sputtering in Ar-D_2 mixture. Fig. 6 shows a combined RBS/NRA spectrum for the film deposited during 67 min on the MgO substrate, resulting in a film thickness of 255 nm, as estimated with the determined film density. The presence of 5.3×10^{15} D/cm^2 has been measured by NRA (statistical uncertainty of 10%), corresponding to 0.28% of the atomic content in the film. Such retention value is judged to be low. It indicates low affinity of sputtered and then deposited material towards incorporation of low energy deuterium molecules, atoms and ions. To obtain the depth information and to access possible deuterium loss by isotopic exchange under air exposure, ERDA measurements were performed in a film deposited under similar conditions using H_2 instead of D_2 (Fig. 6). The presence of hydrogen at the surface of the samples is detected in both cases: 9×10^{15} H/cm^2 and 10×10^{15} H/cm^2 for films produced in Ar + H_2 and Ar + D_2, respectively. The H presence is mainly attributed to the adsorption of water and hydrocarbons from air exposure. The presence of deuterium from the sample surface up to the probing depth of the analysis is confirmed for the Ar + D_2 sample. The probing depth for deuterium was estimated from SIMNRA simulation to be ~100 nm of the film considering the energy from which the deuterium signal overlaps with the hydrogen signal. The atomic D content in films as obtained from ERDA is 0.20% being in a good agreement with the NRA data. For deeper regions of the film, H and D were homogenously distributed with an atomic content of 0.51% and 0.65% for Ar + H_2 and Ar + D_2 samples, respectively. A SIMNRA simulation considering a target with D homogeneously distributed in the film is presented in Fig. 6 (right, inset) in comparison to the experimental data. A discrepancy between experimental and simulated data close to the surface indicates the D deficiency in this region. It can be attributed to desorption or H-D isotope exchange during the exposure to air. Nonetheless, the data coherently indicate that the content of hydrogen isotopes in the films does not exceed 1 at. %, i.e. it is on a low level. Low retention of D in RAFMs and Fe exposed to deuterium containing plasma in comparison to other PFC such as tungsten was already previously reported and attributed to the relatively low concentration of strong trapping sites from intrinsic defects in comparison to, for example, W or irradiated RAFMs [45–46]. One might notice that further thermal desorption spectroscopy studies would be needed to better understand the nature of the traps formed in the deposited films. Nevertheless, the present results show that this relatively low retention of deuterium also applies to deposited materials with significantly different micro- and nanostructure.

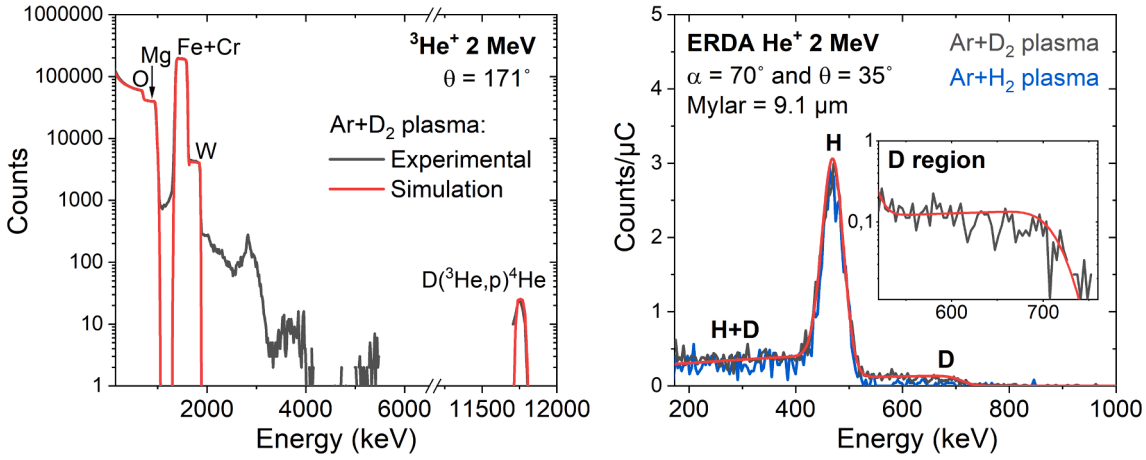

Fig. 6. (left) RBS and NRA spectrum for a EUROFER 97 deposited film on MgO for 67 min under Ar and D_2 atmosphere and (right) ERDA spectra for films grown in the indicated conditions. Inset shows the D region for Ar + D_2 plasma sample (black line) in comparison to SIMNRA simulation considering a homogeneous distribution of deuterium in the film (red line). (For interpretation of the references to colour in this figure legend, the reader is referred to the web version of this article.)

4. Summary and conclusion

The formation of sputter-deposited films from EUROFER97 was investigated and the composition, microstructure, and mechanical properties were compared to its bulk counterpart. Although bulk and thin films presented similar composition, significant lower density and higher hardness was observed in the films. On the other hand, thin films presented high resistance to deuterium retention, when deposition was performed in a mix of argon and deuterium. The study constitutes a first-ever approach to the global characterization of sputtered EUROFER97, and to the assessment of hydrogen isotope (both H and D) retention in deposited metallic films. While the laboratory experiments exhibit limited comparability to the fusion reactor environment, this work is a clear step towards understanding the composition and fuel retention in re-deposited/co-deposited layers that might be formed in deposition zones on PFC and probably also in remote areas of a reactor. The composition of co-deposits may reflect the bulk composition of the alloy, because the wall will be eroded not only by hydrogen isotopes (D and tritium) but also by heavier species originally removed from PFC, i.e. heavy species which will sputter high-Z metals like W. The results indicate that fuel retention in steel-based co-deposits may be expected to be low. This would be anticipated if carbon and oxygen impurity fluxes in a reactor are low, i.e. no significant leaks and low level of intrinsic C impurities in wall materials. The present study breaks the ground for a series of potential investigations of re-deposited films from low-activation steels as likely being formed on plasma facing components of future fusion devices. At first, further experiments detailing the effects of plasma composition on re-deposition can be conducted. In parallel, sputter yields from the deposited films, fuel retention, thermal stability to segregation as well as studies of energy deposition can be conducted.

CRediT authorship contribution statement

E. Pitthan: Conceptualization, Methodology, Investigation, Formal analysis, Visualization, Writing – original draft, Project administration. **P. Petersson:** Conceptualization, Methodology, Resources, Investigation, Writing – review & editing. **T.T. Tran:** Investigation, Formal analysis, Visualization, Writing – review & editing. **D. Moldarev:** Investigation, Formal analysis, Visualization, Writing – review & editing. **R. Kaur:** Investigation, Writing – review & editing. **J. Shams-Latifi:** Methodology, Writing – review & editing. **P. Ström:** Conceptualization, Investigation, Writing – review & editing. **M. Hans:** Investigation, Formal analysis, Writing – review & editing. **M. Rubel:** Conceptualization, Resources, Writing – review & editing, Supervision. **D. Primetzhofer:** Conceptualization, Resources, Writing – review & editing, Supervision, Project administration, Funding acquisition.

Declaration of Competing Interest

The authors declare that they have no known competing financial interests or personal relationships that could have appeared to influence the work reported in this paper.

Data availability

Data will be made available on request.

Acknowledgements

This work has been carried out within the framework of the EUROfusion Consortium, funded by the European Union via the Euratom Research and Training Programme (Grant Agreement No 101052200 — EUROfusion). Views and opinions expressed are however those of the author(s) only and do not necessarily reflect those of the European Union or the European Commission. Neither the European Union nor the European Commission can be held responsible for them. Accelerator operation was supported by the Swedish Research Council VR-RFI, contracts #2019_00191, and the Swedish Foundation for Strategic Research (SSF) under contract RIF14-0053.

References

[1] S. Brezinsek, et al., Plasma–wall interaction studies within the EUROfusion consortium: progress on plasma-facing components development and qualification, Nucl. Fusion 57 (2017), 116041.
[2] H. Bolt, V. Barabash, G. Federici, J. Linke, A. Loarte, J. Roth, K. Sato, Plasma facing and high heat flux materials – needs for ITER and beyond, J. Nucl. Mater. 307–311 (2002) 43–52.
[3] R. Schäublin, A. Ramar, N. Baluc, V. de Castro, M.A. Monge, T. Leguey, N. Schmid, C. Bonjour, Microstructural development under irradiation in European ODS ferritic/martensitic steels, J. Nucl. Mater. 351 (2006) 247–260.
[4] T. Loarer, Fuel retention in tokamaks, J. Nucl. Mater. 390–391 (2009) 20–28.
[5] P. Ström, P. Petersson, M. Rubel, D. Primetzhofer, S. Brezinsek, A. Kreter, B. Unterberg, G. Sergienko, K. Sugiyama, Ion beam analysis of tungsten layers in EUROFER model systems and carbon plasma facing components, Nucl. Inst. Methods Phys. Res. B 371 (2016) 355–359.
[6] H.R. Koslowski, S.R. Bhattacharyya, P. Hansen, C.h. Linsmeier, M. Rasiński, P. Ström, Temperature-dependent in-situ LEIS measurement of W surface enrichment by 250 eV D sputtering of EUROFER, Nucl. Mater. Energy 16 (2018) 181–190.
[7] P. Ström, P. Petersson, R.A. Parra, M. Oberkofler, T. Schwarz-Selinger, D. Primetzhofer, Sputtering of polished EUROFER97 steel: Surface structure modification and enrichment with tungsten and tantalum, J. Nucl. Mater. 508 (2018) 139–146.
[8] R. Arredondo, M. Balden, A. Mutzke, U. von Toussaint, S. Elgeti, T. Höschen, K. Schlueter, M. Mayer, M. Oberkofler, W. Jacob, Impact of surface enrichment and morphology on sputtering of EUROFER by deuterium, Nucl. Mater. Energy 23 (2020), 100769.
[9] M. Rasiński, A. Kreter, S. Möller, T. Schlummer, Y. Martynova, S. Brezinsek, C. h. Linsmeier, The microstructure of reduced activation ferritic/martensitic (RAFM) steels exposed to D plasma with different seeding impurities, Phys. Scr. T170 (2017), 014036.
[10] M. Mayer, T.F. Silva, R. Arredondo, M. Balden, I. Bogdanović-Radović, T. Höschen, H. Maier, M. Oberkofler, L. Ru, Z. Siketić, Tungsten surface enrichment in EUROFER and Fe-W model systems studied by high-resolution time-of-flight Rutherford backscattering spectroscopy, Nucl. Mater. Energy 17 (2018) 147–151.
[11] P. Ström, D. Primetzhofer, In-situ measurement of diffusion and surface segregation of W and Ta in bare and W-coated EUROFER97 during thermal annealing, Nucl. Mater. Energy 27 (2021), 100979.
[12] J. Shams-Latifi, P. Ström, E. Pitthan, D. Primetzhofer, An in-situ ToF-LEIS and AES study of near-surface modifications of the composition of EUROFER97 induced by thermal annealing, Nucl. Mater. Energy 30 (2022), 101139.
[13] J. Roth, K. Sugiyama, V. Alimov, T. Höschen, M. Baldwin, R. Doerner, EUROFER as wall material: Reduced sputtering yields due to W surface enrichment, J. Nucl. Mater. 454 (2014) 1–6.
[14] M. Reinhart, S. Möller, A. Kreter, M. Rasinski, B. Kuhn, Influence of surface temperature, ion impact energy, and bulk tungsten content on the sputtering of steels: In situ observations from plasma exposure in PSI-2, Nucl. Mater. Energy 33 (2022), 101244.
[15] K. Sugiyama, M. Balden, S. Elgeti, T. Höschen, M. Oberkofler, J. Roth, W. Jacob, Erosion of EUROFER steel by mass-selected deuterium ion bombardment, Nucl. Mater. Energy 16 (2018) 114–122.
[16] P. Ström, D. Primetzhofer, T. Schwarz-Selinger, K. Sugiyama, Compositional and morphological analysis of FeW films modified by sputtering and heating, Nucl. Mater. Energy 12 (2017) 471–477.
[17] R. Stadlmayr, P.S. Szabo, B.M. Berger, C. Cupak, R. Chiba, D. Blöch, D. Mayer, B. Stechauner, M. Sauer, A. Foelske-Schmitz, M. Oberkofler, T. Schwarz-Selinger, A. Mutzke, F. Aumayr, Fluence dependent changes of surface morphology and sputtering yield of iron: Comparison of experiments with SDTrimSP-2D, Nucl. Inst. Methods Phys. Res. B 430 (2018) 42–46.
[18] C. Cupak, P.S. Szabo, H. Biber, R. Stadlmayr, C. Grave, M. Fellinger, J. Brötzner, R. A. Wilhelm, W. Möller, A. Mutzke, M.V. Moro, F. Aumayr, Sputter yields of rough surfaces: Importance of the mean surface inclination angle from nano- to microscopic rough regimes, Appl. Surf. Sci. 570 (2021), 151204.
[19] F. Aumayr, P. Bauer, D. Semrad, Accuracy of stopping cross section determination from RBS-spectra by Warters' method, Nucl. Instrum. Methods Phys. Res. 212 (1983) 529–532.
[20] D. Goebl, K. Khalal-Kouache, D. Roth, E. Steinbauer, P. Bauer, Energy loss of low-energy ions in transmission and backscattering experiments, Phys. Rev. A 88 (2013), 032901.
[21] P. Bauer, R. Golser, D. Semrad, P. Maier-Komor, F. Aumayr, A. Arnau, Influence of the chemical state on the stopping of protons and He-ions in some oxides, Nucl. Inst. Methods Phys. Res. B 136–138 (1998) 103–108.
[22] T.T. Tran, L. Jablonka, B. Bruckner, S. Rund, D. Roth, M.A. Sortica, P. Bauer, Z. Zhang, D. Primetzhofer, Electronic interaction of slow hydrogen and helium ions with nickel-silicon systems, Phys. Rev. A 100 (2019), 032705.
[23] P. Ström, D. Primetzhofer, Ion beam tools for nondestructive in-situ and in-operando composition analysis and modification of materials at the Tandem Laboratory in Uppsala, J. Instrum. 17 (2022) P04011.

[24] M. Mayer, SIMNRA, a simulation program for the analysis of NRA, RBS and ERDA, AIP Conference Proceedings 475 (1999) 541–544.
[25] P. Ström, P. Petersson, M. Rubel, G. Possnert, A combined segmented anode gas ionization chamber and time-of-flight detector for heavy ion elastic recoil detection analysis, Rev. Sci. Instrum. 87 (2016), 103303.
[26] M. Janson, CONTES conversion of time-energy spectra—A program for ERDA data analysis User manual, 2004.
[27] B. Wielunska, M. Mayer, T. Schwarz-Selinger, U. von Toussaint, J. Bauer, Cross section data for the D(^{3}He, p)4He nuclear reaction from 0.25 to 6 MeV, Nucl. Inst. Methods Phys. Res. B 371 (2016) 41–45.
[28] A.F. Gurbich, SigmaCalc recent development and present status of the evaluated cross-sections for IBA, Nucl. Inst. Methods Phys. Res. B 371 (2016) 27–32.
[29] F. Besenbacher, I. Stensgaard, P. Vase, Absolute cross section for recoil detection of deuterium, Nucl. Inst. Methods Phys. Res. B 15 (1986) 459–463.
[30] P. Ström, P. Petersson, M. Rubel, E. Fortuna-Zaleśna, A. Widdowson, G. Sergienko, J.E.T. Contributors, Analysis of deposited layers with deuterium and impurity elements on samples from the divertor of JET with ITER-like wall, J. Nucl. Mater. (2019) 202–213.
[31] D. Nečas, P. Klapetek, Gwyddion: an open-source software for SPM data analysis, Cent. Eur. J. Phys. 10 (2012) 181–188.
[32] W.C. Oliver, G.M. Pharr, An improved technique for determining hardness and elastic modulus using load and displacement sensing indentation experiments, J. Mater. Res. 7 (1992) 1564–1583.
[33] S. Knitel, P. Spätig, T. Yamamoto, H.P. Seifert, Y. Dai, G.R. Odette, Evolution of the tensile properties of the tempered martensitic steel Eurofer97 after spallation irradiation at SINQ, Nucl. Mater. Energy 17 (2018) 69–77.
[34] A. Puype, L. Malerba, N. De Wispelaere, R. Petrov, J. Sietsma, Effect of processing on microstructural features and mechanical properties of a reduced activation ferritic/martensitic EUROFER steel grade, J. Nucl. Mater. 494 (2017) 1–9.
[35] E. Gaganidzea, F. Gillemot, I. Szenthe, M. Gorleyc, M. Rietha, E. Diegele, Development of EUROFER97 database and material property handbook, Fusion Eng. Des. 135 (2018) 9–14.
[36] G. Stornelli, A. Di Schino, S. Mancini, R. Montanari, C. Testani, A. Varone, Grain Refinement and Improved Mechanical Properties of EUROFER97 by Thermo-Mechanical Treatments, Appl. Sci. 11 (2021) 10598.
[37] S.R. Kappaganthu, Y. Sun, Studies of structure and morphology of sputter-deposited stainless steel–nitrogen films, Appl. Phys. A 81 (2005) 737–744.
[38] C. Zhou, T. Li, X. Wei, B. Yan, Effect of the Sputtering Power on the Structure, Morphology and Magnetic Properties of Fe Films, Metals 10 (2020) 896.
[39] M. Samuelsson, D. Lundin, J. Jensen, M.A. Raadu, J.T. Gudmundsson, U. Helmersson, On the film density using high power impulse magnetron sputtering, Surf. Coat. Technol. 205 (2010) 591–596.
[40] J.R. Ares, A. Pascual, I.J. Ferrer, C. Sánchez, Grain and crystallite size in polycrystalline pyrite thin films, Thin Solid Films 480–481 (2005) 477–481.
[41] Z. Lu, R.G. Faulkner, N. Riddle, F.D. Martino, K. Yang, Effect of heat treatment on microstructure and hardness of Eurofer 97, Eurofer ODS and T92 steels, J. Nucl. Mater. 386–388 (2009) 445–448.
[42] M. Roldán, P. Fernández, J. Rams, D. Jiménez-Rey, C.J. Ortiz, R. Vila, Effect of helium implantation on mechanical properties of EUROFER97 evaluated by nanoindentation, J. Nucl. Mater. 448 (2014) 301–309.
[43] S. Inoue, T. Saeki, H. Uchida, K. Koterazawa, M. Iwasa, Effects of ion flux on the properties of dc magnetron-sputtered stainless steel films, Vacuum 66 (2002) 257–261.
[44] S. Zak, C.O.W. Trost, P. Kreiml, M.J. Cordill, Accurate measurement of thin film mechanical properties using nanoindentation, J. Mater. Res. 37 (2022) 1373–1389.
[45] Y. Martynova, S. Möller, M. Rasiński, D. Matveev, M. Freisinger, K. Kiss, A. Kreter, B. Unterberg, S. Brezinsek, C.h. Linsmeier, Deuterium retention in RAFM steels after high fluence plasma exposure, Nucl. Mater. Energy 12 (2017) 648–654.
[46] O.V. Ogorodnikova, Z. Harutyunyan, Y.u. Gasparyan, V. Efimov, Helium and deuterium retention in Eurofer97 under sequential irradiation at low fluxes, J. Nucl. Mater. 568 (2022), 153871.